Stability of Fluorine-Free $CaO-SiO_2-Al_2O_3-B_2O_3-Na_2O$ Mold Fluxes

LIN WANG, JIANQIANG ZHANG, YASUSHI SASAKI, OLEG OSTROVSKI, CHEN ZHANG, and DEXIANG CAI

B_2O_3 and Na_2O are key components of fluorine-free mold fluxes for continuous casting, but both are highly volatile, which affects the flux stability. This paper investigated the evaporation of the $SiO_2-CaO-Al_2O_3-B_2O_3-Na_2O$ fluxes (Na_2O: 6 to 10 wt pct, CaO/SiO_2 ratio: 0.8 to 1.3) in the temperatures ranging from 1573 K to 1673 K (1300 °C to 1400 °C) using thermogravimetric analysis. The weight loss as a result of the flux evaporation increased with the increasing temperature for all fluxes. The rate of evaporation was found to be very small for the Na_2O-free flux but significantly increased with the addition of Na_2O. The high evaporation rate of fluxes in the presence of B_2O_3 and Na_2O was attributed to the formation of highly volatile $NaBO_2$. Changing the ratio of CaO/SiO_2, however, did not affect the rate of evaporation. Kinetic analysis of the evaporation processes demonstrated that external mass transfer contributed to the rate of evaporation.

DOI: 10.1007/s11663-016-0907-3

I. INTRODUCTION

THE development of fluorine-free mold fluxes is important for decreasing environmental impact, equipment corrosion, and health hazards brought about by the presence of fluorine in the conventional mold fluxes.[1–4] Many trials have been conducted to replace fluorides with other components.[1–3,5,6] It was suggested that the combination of B_2O_3 and Na_2O is an appropriate substitute for CaF_2, providing low viscosity and melting temperature, and acceptable crystallization and heat transfer of mold fluxes.[2,7,8] However, high volatility of sodium- and boron-containing compounds can be a limitation in the industrial use of the Na_2O-containing boracic fluxes.[9–12] The CaO/SiO_2 ratio is an important characteristic of mold fluxes used in industry, because it is correlated with flux thermophysical properties such as crystallization,[13–15] heat transfer,[16–18] melting properties, and viscosity.[1,5,19,20] It was also reported that CaO/SiO_2 ratio affects the flux evaporation because of the alteration of flux viscosity and the diffusion process in the molten flux.[10,11] The evaporation of high-volatile components changes the chemical compositions of mold fluxes, and thus their physicochemical properties. The changes of mold flux properties can lead to unstable heat transfer and insufficient lubrication, resulting in severe surface defects, *e.g.,* cracks and depressions.[21] Thus, knowledge of kinetics and mechanism of evaporation of mold fluxes containing both B_2O_3 and Na_2O is important for the development of the fluorine-free mold fluxes. However, limited publications in this area showed that the evaporation is very complex, depending on the flux composition and temperature, and the mechanism of the evaporation has not been established.

The purpose of this work is to study the evaporation of $CaO-SiO_2-Al_2O_3-B_2O_3-Na_2O$ mold fluxes using thermogravimetric analysis (TGA), focusing on the effects of the Na_2O content and CaO/SiO_2 ratio.

II. EXPERIMENTAL PROCEDURE

A. *Flux Preparation*

Flux samples were prepared using chemical reagents of $CaCO_3$, Na_2CO_3, SiO_2, Al_2O_3, MgO, and B_2O_3 powders. The mixture of components was ground in an agate mortar for 20 minutes, and then placed in a high-purity graphite crucible. After heating and melting at 1673 K (1400 °C), and holding at this temperature for 20 minutes, the flux was poured onto a steel plate and cooled to room temperature. Subsequently, the flux samples were crushed and ground to fine powders. Compositions of fluxes were analyzed by inductively coupled plasma (ICP) for B_2O_3 and X-ray fluorescence (XRF) for other oxides; the results are listed in Table I. This table also includes the liquidus temperatures (T_{liq}) of fluxes calculated using thermochemical software FactSage 7.0 and their viscosity values (η) reported elsewhere.[22] Fluxes 1, 4, 5, and 6 have varied Na_2O contents from 0 to 9.1 wt pct at a fixed CaO/SiO_2 ratio of 1.3, while Fluxes 2, 3, and 5 have varied CaO/SiO_2 ratios from 0.8 to 1.3 at Na_2O contents close to 8 wt pct. A typical industrial fluorine-containing flux (C) for continuous casting of low-carbon steel was also measured for a comparison.

LIN WANG, JIANQIANG ZHANG, YASUSHI SASAKI, and OLEG OSTROVSKI are with the School of Materials Science and Engineering, UNSW Australia, Sydney, 2052, Australia. Contact e-mail: j.q.zhang@unsw.edu.au CHEN ZHANG and DEXIANG CAI are with the Steelmaking Research Department, Baosteel Group Corporation Research Institute, Shanghai, 201900, China.

Manuscript submitted October 11, 2016.
Article published online January 3, 2017.

B. *Thermogravimetric Measurement*

The evaporation experiments were conducted using a STA449-F1 calorimeter (NETZSCH Instruments, Germany) in the isothermal mode at 1573 K, 1598 K, 1623 K, and 1673 K (1300 °C, 1325 °C, 1350 °C, and 1400 °C) in Ar atmosphere. Not all temperatures were applied for all samples due to the limitation on using the apparatus for high-temperature experiments. The Pt/Rh crucible with 6-mm inner diameter and a volume of 84 μL was employed as the container for the flux. The flux sample for each measurement was approximately 30 mg.

The chamber was evacuated and purged with Ar gas for 300 seconds to ensure a steady gas flow. The sample was then heated to a preset temperature with a heating rate of 50 K/minute, the maximum heating rate for the apparatus. The gas-flow rate was kept constant at 70 mL/minute for the duration of the experiment, which was maximum gas flow rate possible in the measurement. The sample was kept at the experimental temperature for 60 minutes. During the experiment, the weight change of the sample was recorded every 0.1 seconds. Repeated experiments for some selected fluxes demonstrated a good reproducibility of the measurements (Figure 1).

III. RESULTS

A. *Weight Loss Measurement*

Figures 2 and 3 show the influences of temperature and Na_2O content on weight losses of the fluxes (CaO/SiO_2 ratio fixed at 1.3), respectively. The weight loss was characterized by $\Delta m/m_0$, where Δm is the weight change, g; and m_0 is the initial sample weight, g. The evaporation of the industrial fluorine-containing Flux C at 1623 K (1350 °C) was also measured and compared with the fluorine-free mold fluxes in Figure 3(c). The fluorine-containing flux showed much higher weight loss than fluorine-free fluxes at 1623 K (1350 °C) (Figure 3(c)).

In general, the weight loss increased with the increasing temperature (Figure 2). For the Na_2O-free mold flux, the weight loss was much smaller than that for the Na_2O-containing fluxes, less than 0.005 pct at all temperatures for 1 h (Figures 2(a), 3(a), 3(c), and 3(d)). Adding 6.2 wt pct Na_2O significantly increased the rate of flux evaporation (Figures 3(a) and 3(c)). Increasing the Na_2O content from 6.2 to 7.9 wt pct only slightly increased the rate of evaporation (Figures 3(a) through 3(c)). When the content of Na_2O was increased from 7.9 to 9.1 wt pct, there was almost no change in the evaporation rate at 1573 K (1300 °C) (Figure 3(a)), a slightly increased rate at 1350°C (Figure 3(c)), and an early increase but obvious slowdown after 1000 seconds at 1673 K (1400 °C) (Figures 2(d) and 3(d)). As a result, the weight loss at 1673 K (1400 °C) for the flux with 9.1 wt pct Na_2O was even smaller than that at 1623 K (1350 °C) after 1 h of isothermal process (Figure 2(d)).

Figure 4 shows the weight loss of fluxes with a fixed Na_2O content at approximately 8 wt pct but varied CaO/SiO_2 ratios from 0.8 to 1.3 at 1300 °C. An increase in the CaO/SiO_2 ratio from 0.8 to 1.3 had a minor influence on the weight loss.

B. *Evaporation Rate and Activation Energy*

Evaporation changed the slag chemical composition and as a result affected the evaporation rate in the process of measurements. To mitigate this effect, the evaporation rates were analyzed in the first 10 minutes of the TGA measurements. Evaporation rate k, s^{-1}, was calculated as:

$$k = -\frac{\Delta m_i/m_0}{t_i} \quad [1]$$

$$\Delta m_i = m_i - m_0 \quad [2]$$

where $\Delta m_i/m_0$ is the flux mass change, and m_i, g, is the flux mass at time t_i, s. Table II shows the calculated evaporation rates of different fluxes. The evaporation rate changed only slightly with the increasing CaO/SiO_2 ratio at the fixed Na_2O content (Fluxes 2, 3, 5), while it increased with increasing the Na_2O content at the fixed CaO/SiO_2 ratio of 1.3 (Fluxes 1, 4 to 6). The apparent activation energies for the evaporation process were estimated from the Arrhenius plots using data on k obtained at different temperatures:

$$\ln k = \ln A + \frac{E_a}{RT} \quad [3]$$

where A is the preexponential factor; E_a is the apparent activation energy, kJ/mol; R is the gas constant, 8.314 J/(mol·K); and T is the absolute temperature, K.

Table I. Chemical Compositions of Fluxes (wt pct), Their Liquidus Temperatures (K (°C)) Calculated using FactSage and Viscosity (Pa·s) Measured at 1673 K (1400 °C).[22]

Flux No.	CaO/SiO_2	CaO	SiO_2	Al_2O_3	B_2O_3	Na_2O	MgO	Li_2O	CaF_2	T_{liq}, K (°C)	η, Pa·s
1	1.3	51.1	39.2	3.2	6.4	0	0	0	0	1644 (1371)	0.38
2	0.8	36.8	44.9	3.5	6.6	8.2	0	0	0	1565 (1292)	0.29
3	1.0	40.5	40.8	3.6	6.7	8.4	0	0	0	1529 (1256)	0.20
4	1.3	47.2	36.4	3.6	6.6	6.2	0	0	0	1535 (1262)	0.15
5	1.3	46.2	35.7	3.5	6.7	7.9	0	0	0	1514 (1241)	0.17
6	1.3	45.3	35.3	3.8	6.5	9.1	0	0	0	1500 (1227)	0.13
C	0.9	34.5	37.5	3	0	12.5	2.5	0.5	8.5	—	—

—No data available.

Values of E_a are obtained from the slope of ln$k$ *vs* $1/T$ (shown in Figure 5) and listed in Table III. Addition of 6.2 wt pct Na_2O to the $CaO\text{-}SiO_2\text{-}Al_2O_3\text{-}B_2O_3$ system significantly decreased E_a. A further increase in the Na_2O content from 6.2 to 9.1 wt pct had a minor effect on E_a.

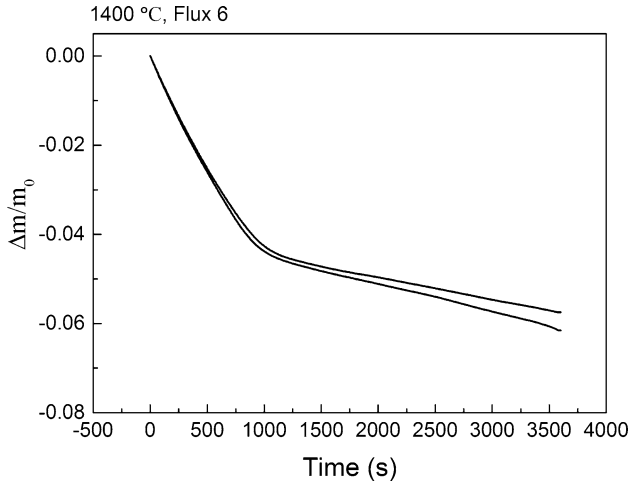

Fig. 1—Repeated weight loss measurements of Flux 6 at 1673 K (1400 °C).

IV. DISCUSSION

Vaporization of fluorine-free fluxes observed in this work was also reported in other works.[10–12,24] Evaporation rate of B_2O_3-containing fluorine-free fluxes depended on the temperature and the flux composition. Increasing the reaction temperature enhanced the flux evaporation. Adding Na_2O into the B_2O_3-containing mold flux significantly increased the rate of flux evaporation. However, varied CaO/SiO_2 ratios at the fixed Na_2O content had no significant effect on the vaporization. The mechanisms, kinetics of evaporation, and the rate-controlling steps are discussed in this paper.

A. *Evaporation Process*

Experimental temperatures in a study of Na_2O-containing fluxes in this work were higher than the liquidus temperatures calculated using FactSage (shown in Table I). The calculated liquidus temperature for the Na_2O-free flux (Flux 1) was higher than 1300 °C, but in situ observation using a hot thermocouple technique[15,25] showed that, at 1300 °C, this flux was in the liquid state. Therefore, all fluxes were liquid at the experimental temperatures. The silicate-based mold fluxes have complex network structures. In the molten

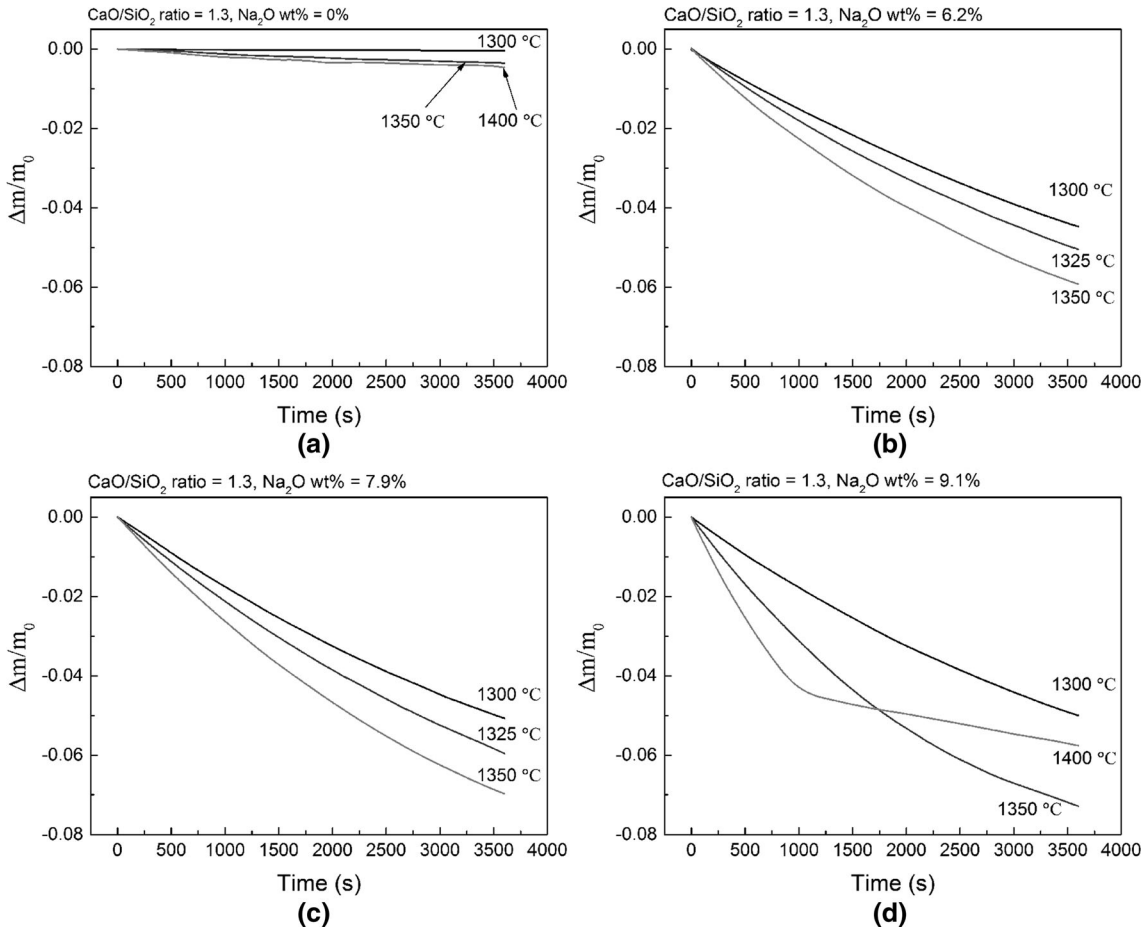

Fig. 2—The weight losses of fluxes with varied Na_2O contents of (*a*) 0 wt pct, (*b*) 6.2 wt pct, (*c*) 7.9 wt pct, and (*d*) 9.1 wt pct, as a function of time at different temperatures with CaO/SiO_2 ratio of 1.3.

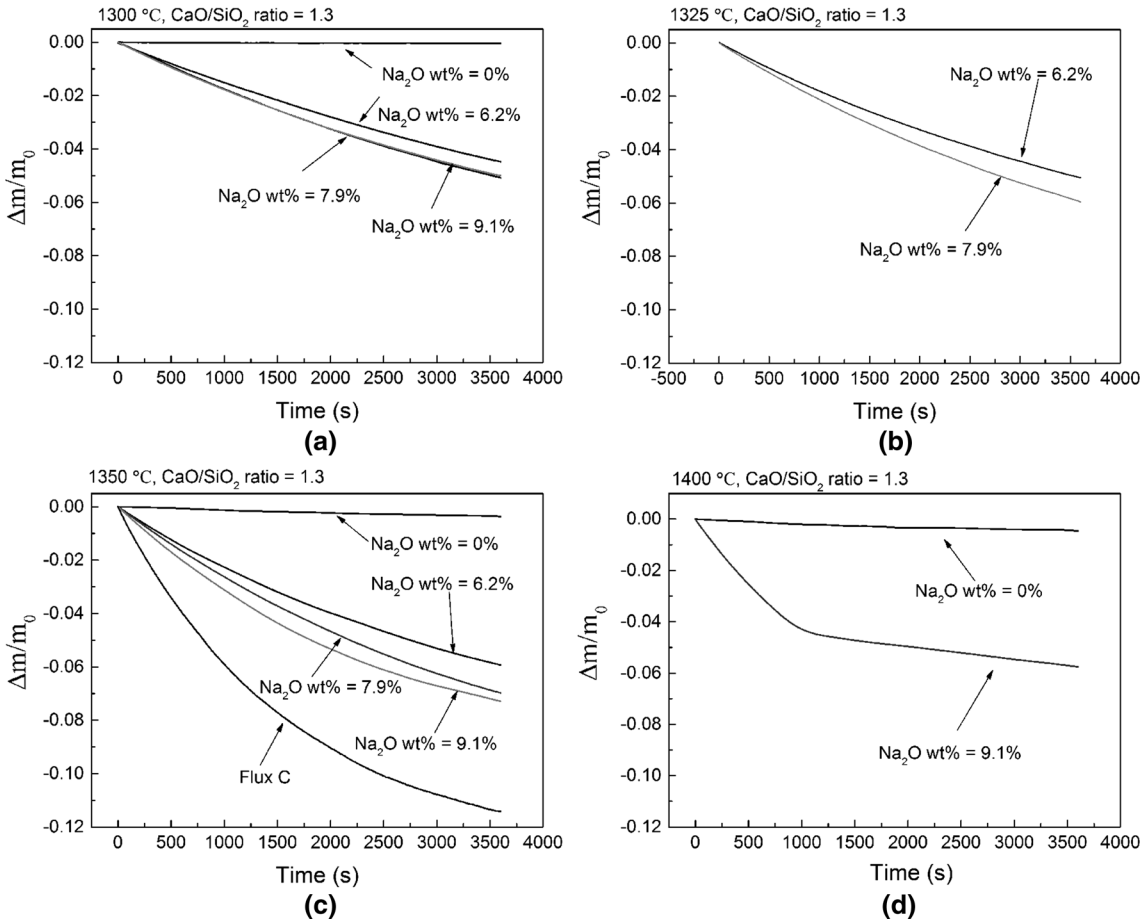

Fig. 3—The influence of Na_2O content on the weight losses of fluxes at different temperatures of (*a*) 1573 K (1300 °C),[23] (*b*) 1598 K (1325 °C), (*c*) 1623 K (1350 °C), and (*d*) 1673 K (1400 °C).[23] (Copyright 2016 by The Minerals, Metals & Materials Society).

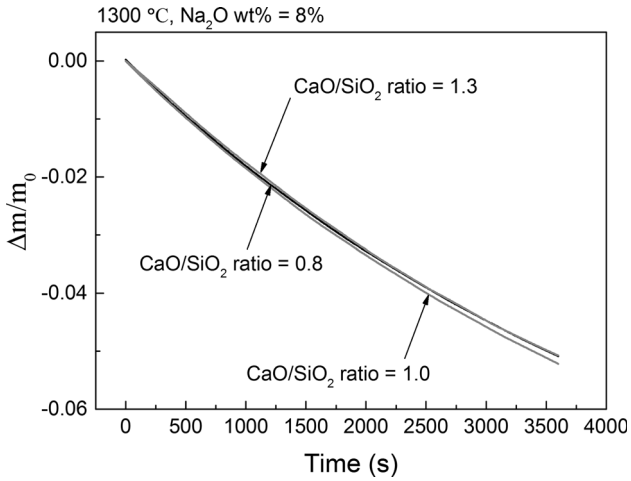

Fig. 4—The influence of CaO/SiO_2 ratio on the weight loss of fluxes at 1573 K (1300 °C).[23] (Copyright 2016 by The Minerals, Metals & Materials Society).

state, oxides form anionic and cationic species. Si-related structures are in the form of different types of anionic tetrahedral units (SiO_2, $Si_2O_5^{2-}$, $Si_2O_6^{4-}$, $Si_2O_7^{6-}$, and SiO_4^{4-}) in the melt.[26] Cations of Al^{3+} substitute for Si^{4+} to form tetrahedral AlO_4^{5-}, with electric charge compensation by cations of Na^+ or Ca^{2+}.[22] B_2O_3 is partially incorporated into the Si-O-Si network resulting in the Si-O-B structure; it also forms trigonal BO_3^{3-} units.[19,27,28] Na_2O and CaO are typical network-modifying oxides, leading to the breakdown of the network structure.

Thermodynamic analysis using FactSage showed that major components of the gas phase in the equilibrium with fluxes under examination were gaseous $NaBO_2$, Na, O_2, and B_2O_3. Formation of these gaseous species can be presented by the following evaporation reactions:[10–12,29]

$$Na_2O + B_2O_3 = 2NaBO_2(g) \quad [4]$$

$$2Na_2O = 4Na\ (g) + O_2(g) \quad [5]$$

$$B_2O_3 = B_2O_3(g) \quad [6]$$

The evaporated species were transported from the molten flux surface out of the crucible to the main gas stream of Ar. Therefore, as schematically shown in Figure 6, the evaporation process included three main steps:

Table II. Evaporation Rates k (s^{-1}) of Fluxes

Flux No.	1573 K (1300 °C)	1598 K (1325 °C)	1623 K (1350 °C)	1673 K (1400 °C)
1	3.08×10^{-7}	—	8.21×10^{-7}	1.90×10^{-6}
2	1.93×10^{-5}	—	—	—
3	1.93×10^{-5}	—	—	—
4	1.54×10^{-5}	1.90×10^{-5}	2.43×10^{-5}	—
5	1.81×10^{-5}	2.20×10^{-5}	2.89×10^{-5}	—
6	1.87×10^{-5}	—	3.34×10^{-5}	4.91×10^{-5}
C	—	—	6.53×10^{-5}	—

—No evaporation rates measured under these conditions.

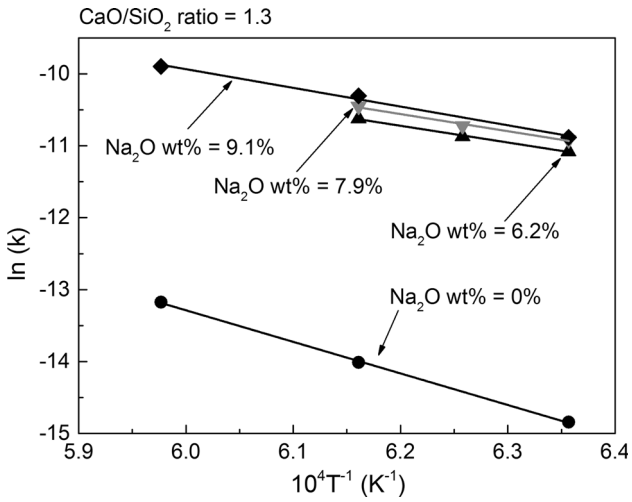

Fig. 5—Arrhenius plots for fluxes with varying Na_2O contents.[23] (Copyright 2016 by The Minerals, Metals & Materials Society).

Table III. Calculated E_a for Fluxes with Different Na_2O Contents

Flux No.	Na_2O, wt pct	E_a, kJ/mol	R^2*
1	0	365	0.99
4	6.2	193	0.99
5	7.9	198	0.98
6	9.1	211	0.98

* R^2 is a statistical measure of how close the data are to the fitted regression line.

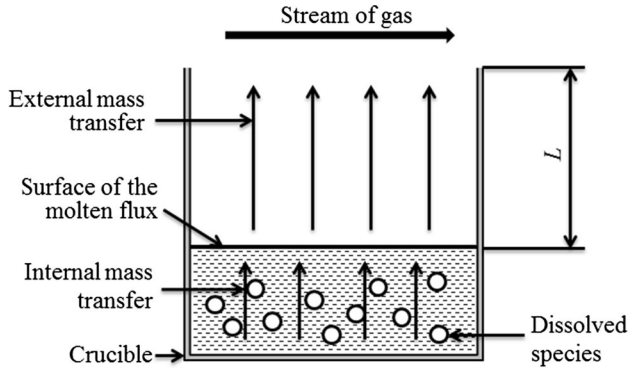

Fig. 6—Schematic of the evaporation process.

(1) Evaporation reactions following Eqs. [4] through [6];
(2) Internal mass transfer of dissolved species to the surface of the molten flux; and
(3) External mass transfer of gaseous species from the flux/gas interface out of the crucible.

B. *Rate-Controlling Steps of Evaporation*

1. *Chemical reaction*

The maximum possible rate of evaporation (free evaporation, s^{-1}) of gaseous species can be calculated using the Hertz–Knudsen equation:[30]

$$k_{\max} = \frac{44.3P_A}{(M_A T)^{0.5}} \cdot \frac{M_A S}{10.1325 m_0} \qquad [7]$$

where P_A is partial pressure of A (A: $NaBO_2$, Na, O_2, or B_2O_3), Pa; S is the surface area of interface, m^2; T is temperature in K; and M_A is molecular weight of A, g/mol.

Table IV shows the equilibrium vapor pressures of major gaseous species for Na_2O-containing fluxes calculated using FactSage. The vapor pressure of $NaBO_2$ is the highest for the Na_2O-containing fluxes, indicating that it is a dominant volatile species. The reaction presented by Eq. [4] is therefore the major reaction for the evaporation in the presence of both Na_2O and B_2O_3.

The maximum rates of evaporation calculated using Eq. [7] are shown in Table V. Calculated $k_{\max}$ are three orders of magnitude higher than the measured evaporation rates k. Therefore, contribution of the chemical reactions to the rate control of the evaporation of the fluxes can be ignored.

2. *Mass transfer in molten flux*

Experimental results showed that the rate of evaporation was not affected by the change of the CaO/SiO_2 ratio at the fixed B_2O_3 and Na_2O contents. As shown in Table I, increasing the CaO/SiO_2 ratio decreases the viscosity of the flux as a result of the flux depolymerization. It can be expected in accordance with Stokes–Einstein equation that diffusion coefficients of flux constituents increase with the increasing CaO/SiO_2 ratio.[31] If the mass transfer in the liquid flux contributed to the evaporation rate control, the evaporation rate would have been affected by the depolymerization of the flux caused by the increasing CaO/SiO_2 ratio. Therefore, it can be concluded that the internal mass

transfer in the liquid phase is not the rate-controlling step in the flux vaporization under experimental conditions in this work. Zhang *et al.*[11] also observed a negligible effect of CaO/SiO_2 ratio from 0.77 to 1.18 on the evaporation of $CaO\text{-}SiO_2\text{-}Al_2O_3\text{-}B_2O_3\text{-}Na_2O\text{-}TiO_2$ mold fluxes. For $CaO\text{-}SiO_2\text{-}Al_2O_3$ flux with high Na_2O content (20 wt pct), Li *et al.*[10] found that the mass transfer in the liquid flux gradually became a rate-controlling step after a long time of the evaporation reaction (from 3500 to 7000 seconds) resulting in the significant decrease of Na_2O concentration. Measurements in this work lasted less than 3600 seconds.

3. *External mass transfer in the gas phase*

In the analysis of the external mass transfer, it is assumed that the evaporation reaction reaches equilibrium and the flux composition remains unchanged. Concentration gradients in the flux are neglected based on the above analysis of the internal mass transfer.

In the measurements, once the evaporation starts, gaseous species evaporate from the interface and leave the system with the carrier Ar gas. After a certain period of time, a steady state is established in which the concentrations of gaseous species in the bulk Ar gas become constant.[32] The fluxes of gaseous species diffusing from the flux/gas interface to the top of a platinum crucible can be obtained by calculating the flux of each gaseous component J_A, mol/second, which is defined as

$$J_A = \frac{\Delta m_A}{t M_A} \quad [8]$$

where Δm_A is the mass loss of component A.

In order to simplify the problem, it is assumed that there is no convection occurring inside the crucible. Then the flux of the component A can be calculated as[10]

$$\frac{J_A}{S} = \frac{\left(P_A^i - P_A^b\right) D_{A-Ar}}{LRT} \quad [9]$$

where i and b indicate the interface and bulk, respectively; and L is a boundary-layer thickness which is assumed to be the distance between the surface of liquid flux and the crucible top, m. L is estimated by assuming that the density of the fluorine-free fluxes is $\rho = 3.05 g/cm^3$. P_A^i and P_A^b are the partial pressures at the interface (equilibrium partial pressure, P_A) and in the bulk gas, respectively. P_A^b in the flowing Ar gas atmosphere is assumed to be zero. D_{A-Ar} is the diffusion coefficient of gaseous species A through Ar gas,

Table IV. Calculated Vapor Pressures P_A (Pa) for Major Gaseous Species

Flux No.	Gaseous Species	1573 K (1300 °C)	1598 K (1325 °C)	1623 K (1350 °C)	1673 K (1400 °C)
2	$NaBO_2$ (g)	56.45	76.57	102.61	178.13
	Na (g)	0.52	0.76	1.10	2.24
	O_2 (g)	0.13	0.18	0.27	0.55
	B_2O_3 (g)	6.42×10^{-3}	1.07×10^{-2}	1.73×10^{-2}	4.33×10^{-2}
3	$NaBO_2$ (g)	60.86	82.25	109.83	189.46
	Na (g)	0.82	1.19	1.71	3.42
	O_2 (g)	0.20	0.30	0.42	0.85
	B_2O_3 (g)	2.87×10^{-3}	4.79×10^{-3}	7.82×10^{-3}	1.98×10^{-2}
4	$NaBO_2$ (g)	46.85	62.98	83.67	143.03
	Na (g)	0.97	1.41	2.01	3.99
	O_2 (g)	0.24	0.35	0.50	0.99
	B_2O_3 (g)	1.36×10^{-3}	2.27×10^{-3}	3.71×10^{-3}	9.43×10^{-3}
5	$NaBO_2$ (g)	58.37	78.42	104.16	177.96
	Na (g)	1.38	1.99	2.84	5.60
	O_2 (g)	0.34	0.50	0.71	1.39
	B_2O_3 (g)	1.02×10^{-3}	1.72×10^{-3}	2.82×10^{-3}	7.24×10^{-3}
6	$NaBO_2$ (g)	61.89	83.15	110.43	188.66
	Na (g)	1.72	2.48	3.53	6.93
	O_2 (g)	0.43	0.62	0.88	1.72
	B_2O_3 (g)	7.74×10^{-4}	1.30×10^{-3}	2.14×10^{-3}	5.54×10^{-3}

Table V. Maximum Evaporation Rates k_{max} (s^{-1}) for Fluxes

Flux No.	1573 K (1300 °C)	1598 K (1325 °C)	1623 K (1350 °C)	1673 K (1400 °C)
2	0.048	0.064	0.086	0.147
3	0.051	0.070	0.092	0.157
4	0.039	0.054	0.070	0.120
5	0.050	0.067	0.087	0.149
6	0.053	0.071	0.095	0.158

cm^2/second, which was calculated by Chapman–Enskog equation:[30]

$$D_{A-Ar} = 0.0018583 \times \frac{T^{3/2}}{P \cdot \sigma^2_{A-Ar} \cdot \Omega_{A-Ar}} \times \left(\frac{1}{M_A} + \frac{1}{M_{Ar}}\right)^{1/2} \quad [10]$$

where P is the pressure, atm; M_A and M_{Ar} are the molecular weights of gaseous species A and Ar, respectively; and Ω_{A-Ar} is the collision integral for diffusion, which is a function of the dimensionless temperature (or reduced temperature) $kT/\varepsilon_{A\text{-}Ar}$.[33]

Parameters σ_{A-Ar}, Å, and ε_{A-Ar}, J, are the parameters of the Lennard-Jones potential which can be estimated from the following equations:[33]

$$\sigma_{A-Ar} = \frac{1}{2}(\sigma_A + \sigma_{Ar}) \quad [11]$$

$$\varepsilon_{A-Ar} = (\varepsilon_A \varepsilon_{Ar})^{1/2} \quad [12]$$

The values $\frac{\varepsilon_{Ar}}{k}$ and σ_{Ar} taken from[33] are 122.4 K and 3.432 Å, respectively. The values of ε_A and σ_A were estimated by the following empirical equations:[33]

$$\frac{\varepsilon_A}{k} = 1.92 T_{m,A} \quad [13]$$

$$\sigma_A = 1.222 V_{m,A}^{\frac{1}{3}} \quad [14]$$

where k is Boltzmann constant, 1.38×10^{-23} J/K; T_m is the melting temperature, K; and $V_{m,A}$ is the molar volume at melting temperature, cm^3/mol. Table VI shows the calculated $\frac{\varepsilon_A}{k}$ and σ_A using Eqs. [13] and [14]. V_m of B_2O_3 was regressed from the temperature dependence of molar volume in Mackenzie's work.[34]

Values of Ω_{A-Ar} for different species, and calculated $\kappa T/\varepsilon_{A\text{-}Ar}$ and D_{A-Ar} values are shown in Table VII.

The rate of total weight loss of the molten flux can be calculated using the following equation:

$$\frac{\Delta m_i}{t_i} = \sum M_A J_A \quad [15]$$

By combining Eqs. [9] and [15], evaporation rate can be estimated from the following equation:

$$-\frac{\Delta m_i / m_0}{t_i} = \frac{S}{RTLm_0} \sum M_A D_{A-Ar} P_A \quad [16]$$

The calculated evaporation rates for different fluxes, compared with the experimental results, are shown in Figure 7. In general, the measured values are lower than the calculated ones, although the difference between them is small. The measured values are close to the calculated ones when the evaporation rate is low. It can be suggested that the diffusion of gaseous phase from the flux surface to the main gas stream contributed to the rate control. For the fluxes with low rate of evaporation, the external mass transfer played a more important role in the rate control than for those with high rate of evaporation. Zhang *et al.*[11] and Li *et al.*[10] in a similar analysis obtained much larger calculated values than the experimental data. Under conditions in their works, vapor pressures of the gaseous species were much higher than those obtained in this work. The gas-phase mass transfer was also reported to contribute

Table VI. Parameters $\frac{\varepsilon_A}{k}$ and σ_A for Different Gaseous Species

Gaseous Species	M_A, g/mol	ρ_{liq}, g/cm^3	V_m, cm^3/mol	T_m, K	$\frac{\varepsilon_A}{k}$, K	σ_A, Å
$NaBO_2$	65.80	2.46	26.70	1239	2378.88	3.653
Na	22.99	0.93	24.72	371	712.32	3.560
O_2	32.00	—	—	—	113[33]	3.433[33]
B_2O_3	69.62	2.46	42.20[34]	723	1388.16	4.254

Table VII. Values of $\kappa T/\varepsilon_{A\text{-}Ar}$, Ω_{A-Ar} and Estimated Diffusion Coefficients of Gaseous Species in Ar Gas (10^{-4} m^2/s)

Parameter	1573 K (1300 °C)	1598 K (1325 °C)	1623 K (1350 °C)	1673 K (1400 °C)
$\kappa T/\varepsilon_{NaBO_2-Ar}$	2.915	2.962	3.008	3.101
Ω_{NaBO_2-Ar}	0.9588	0.9500	0.9500	0.9418
D_{NaBO_2-Ar}	1.933	1.951	2.045	2.159
$\kappa T/\varepsilon_{Na-Ar}$	5.328	5.412	5.497	5.666
Ω_{Na-Ar}	0.8428	0.8428	0.8428	0.8129
D_{Na-Ar}	2.947	2.947	3.089	3.351
$\kappa T/\varepsilon_{O_2-Ar}$	13.376	13.589	13.802	14.227
Ω_{O_2-Ar}	0.7025	0.7025	0.7025	0.7025
D_{O_2-Ar}	2.435	3.323	3.483	3.645
$\kappa T/\varepsilon_{B_2O_3-Ar}$	3.816	3.877	3.938	4.059
$\Omega_{B_2O_3-Ar}$	0.8952	0.8897	0.8897	0.8845
$D_{B_2O_3-Ar}$	1.741	1.751	1.835	1.932

to the rate of evaporation of CaO-SiO_2-Al_2O_3-Na_2O-MgO-CaF_2 mold fluxes at temperatures in the range from 1623 K to 1793 K (1350 °C to 1520 °C),[35] although the major evaporated species from the fluorine-containing fluxes are different from those in the fluorine-free fluxes considered in this work. At a given temperature, the evaporation rate is directly proportional to P_{NaBO_2}. With the increasing Na_2O content, P_{NaBO_2} increases, while the increase in CaO/SiO_2 ratio does not significantly affect P_{NaBO_2}(Table IV). The acceleration effect of Na_2O on the evaporation of B_2O_3-containing fluxes was also reported by others.[29,36]

The rate of evaporation was calculated using data for the first 10-minutes reaction. The rate of evaporation slowed down with the increasing exposure time. As mentioned before, flux evaporation leads to the change of the flux composition, and thus the flux properties, including the rate of evaporation. After a significant decrease in the contents of volatile species, internal mass transfer is expected to play a more significant role. The change of the rate-limiting step for the flux evaporation with the increasing reaction time was reported by Li *et al.*[10]

The effect of exposure time on the flux evaporation becomes more significant at higher temperature. In this work, the apparent descending trend in the weight loss of Flux 6 was observed after 1000 seconds at 1673 K (1400 °C) (Figures 2(d) and 3(d)); it can be attributed to the compositional change by reducing the contents of both boron and sodium in the flux, which may change the flux melting and evaporation properties. Figure 8 shows the variations of the vapor pressure and liquidus temperature as a function of weight loss of Flux 6 calculated using FactSage. In these calculations, only evaporation of $NaBO_2$ was considered. With the increasing flux weight loss, the vapor pressure reduces (Figure 8(a)), and the liquidus temperature rises (Figure 8(b)). Based on the above analysis, the external mass transfer decreases according to Eq. [16], reducing the evaporation rate. When the dimensionless weight loss reached 0.08 pct, the calculated liquidus temperature approached 1673 K (1400 °C). It means that any further weight loss will lead to the solid precipitation which slows down the evaporation kinetics significantly.

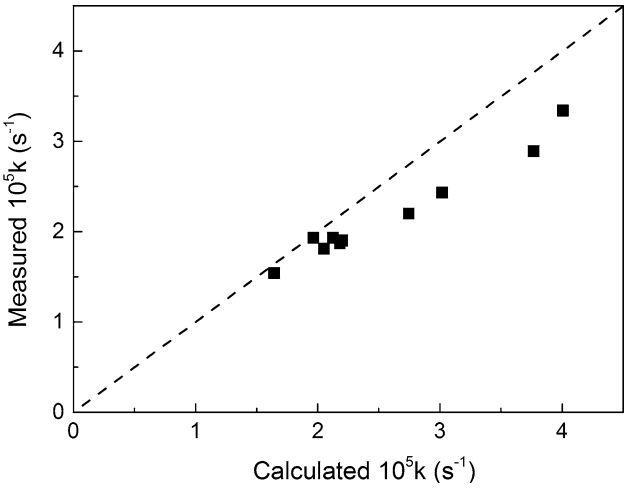

Fig. 7—A comparison of measured and estimated evaporation rates.

V. CONCLUSIONS

The present study of stability of the fluorine-free mold fluxes SiO_2-CaO-Al_2O_3-B_2O_3-Na_2O demonstrated that the evaporation of these fluxes was much slower in comparison with industrial fluorine-containing flux. The rate of the flux evaporation depended on the temperature and the flux composition. The weight loss as a result of the flux evaporation increased with the increasing temperature. The evaporation of the B_2O_3-containing fluxes without Na_2O at temperatures ranging from 1573 K to 1673 K (1300 °C to 1400 °C) was less than 0.005 pct. Significant evaporation was observed when the fluxes contained both B_2O_3 and Na_2O, which was attributed to the formation of the highly volatile $NaBO_2$. The addition of 6.2 wt pct Na_2O increased the flux evaporation at 1623 K (1350 °C) to greater than

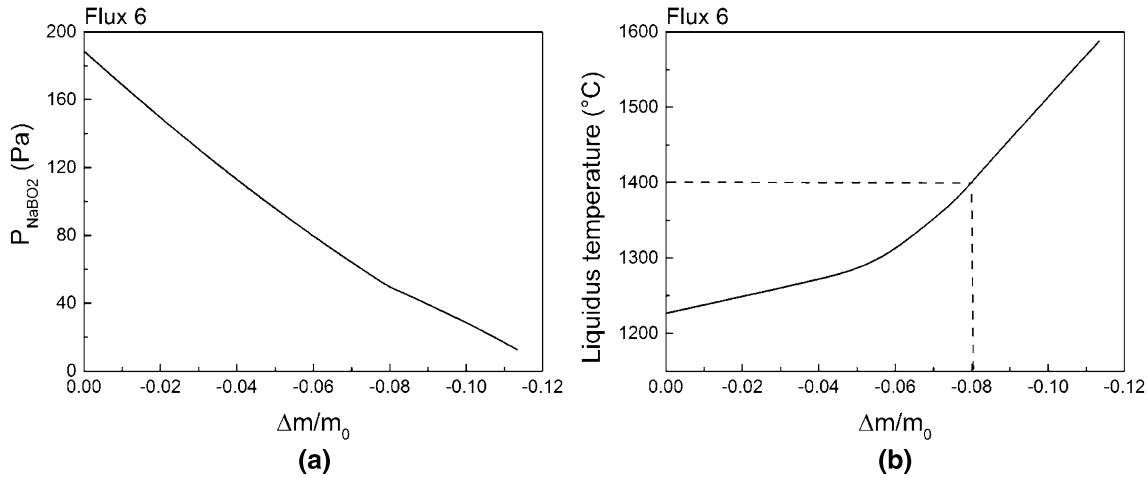

Fig. 8—The influences of weight loss on (*a*) vapor pressure and (*b*) liquidus temperature of Flux 6 calculated using FactSage.

0.06 pct. The increase in the rate of the vaporization slowed down with increasing the Na_2O content further to 9.1 wt pct. Variation of the CaO/SiO_2 ratio, however, did not change the flux evaporation rate.

The flux evaporation process was analyzed by considering chemical reactions and internal and external mass transfers. Major species in the gas phase in the equilibrium with molten fluxes calculated using FactSage included $NaBO_2$, Na, O_2, and B_2O_3. The maximum rate of evaporation reactions, calculated using Hertz–Knudsen equation, was much higher than the measured evaporation rate. The calculated rate of the external mass transfer of the gaseous species from the flux/gas interface to the main gas stream was in reasonable agreement with the measured rate of evaporation. It was concluded that the external mass transfer in the gas phase contributed to the rate control of the flux evaporation.

The flux evaporation leads to the change in the flux composition and flux properties, affecting the evaporation rate.

ACKNOWLEDGMENTS

This project was financially supported by Baosteel through BAJC, Abel Metal, and Australian Research Council (ARC LP130100773).

REFERENCES

1. G.H. Wen, S. Sridhar, P. Tang, X. Qi, and Y.Q. Liu: *ISIJ Int*., 2007, vol. 47, pp. 1117–25.
2. A.B. Fox, K.C. Mills, D. Lever, C. Bezerra, C. Valadares, I. Unamuno, J.J. Laraudogoitia, and J. Gisby: *ISIJ Int*., 2005, vol. 45, pp. 1051–58.
3. J.L. Klug, R. Hagemann, N.C. Heck, A.C.F. Vilela, H.P. Heller, and P.R. Scheller: *Steel Res. Int*., 2012, vol. 83, pp. 1186–93.
4. M. Persson, S. Seetharaman, and S. Seetharaman: *ISIJ Int*., 2007, vol. 47, pp. 1711–17.
5. Z. Wang, Q.F. Shu, and K.C. Chou: *Steel Res. Int*., 2013, vol. 84, pp. 766–76.
6. Z.T. Zhang, G.H. Wen, and Y.Y. Zhang: *Int. J. Miner. Metell. Mater*., 2011, vol. 18, pp. 150–58.
7. S.Y. Choi, D.H. Lee, D.W. Shin, S.Y. Choi, J.W. Cho, and J.M. Park: *J. Non-Cryst. Solids*, 2004, vol. 345, pp. 157–60.
8. C.B. Shi, M.D. Seo, J.W. Cho, and S.H. Kim: *Metall. Mater. Trans. B*, 2014, vol. 45, pp. 1081–97.
9. R.G.C. Beerkens: *J. Am. Ceram. Soc*., 2001, vol. 84, pp. 1952–60.
10. M. Li, T. Utigard, and M. Barati: *Metall. Mater. Trans. B*, 2015, vol. 46, pp. 74–82.
11. Z.T. Zhang, S. Sridhar, and J.W. Cho: *ISIJ Int*., 2011, vol. 51, pp. 80–87.
12. V.L. Stolyarova, G.G. Ivanov, and S.V. Stolyar: *Glass Phys. Chem*., 2002, vol. 28, pp. 112–16.
13. M. Hanao: *ISIJ Int*., 2013, vol. 53, pp. 648–54.
14. J. Li, Z. Zhang, L. Liu, W. Wang, and X. Wang: *ISIJ Int*., 2013, vol. 53, pp. 1696–703.
15. J. Yang, J.Q. Zhang, Y. Sasaki, O. Ostrovski, C. Zhang, D.X. Cai, and Y. Kashiwaya: *ISIJ Int*., 2016, vol. 56, pp. 574–83.
16. L. Zhou, W. Wang, J. Wei, and K. Zhou: *ISIJ Int*., 2015, vol. 55, pp. 821–29.
17. W.L. Wang, K.Z. Gu, L.J. Zhou, F.J. Ma, I. Sohn, D.J. Min, H. Matsuura, and F. Tsukihashi: *ISIJ Int*., 2011, vol. 51, pp. 1838–45.
18. B.X. Lu, W.L. Wang, J. Li, H. Zhao, and D.Y. Huang: *Metall. Mater. Trans. B*, 2013, vol. 44, pp. 365–77.
19. L. Wang, Y. Cui, J. Yang, C. Zhang, D. Cai, J. Zhang, Y. Sasaki, and O. Ostrovski: *Steel Res. Int*., 2015, vol. 86, pp. 670–77.
20. N. Takahira, M. Hanao, and Y. Tsukaguchi: *ISIJ Int*., 2013, vol. 53, pp. 818–22.
21. W.L. Wang, K. Blazek, and A. Cramb: *Metall. Mater. Trans. B*, 2008, vol. 39, pp. 66–74.
22. L. Wang, C. Zhang, D.X. Cai, J. Zhang, Y. Sasaki, and O. Ostrovski: *Metall. Mater. Trans. B*, 2016, DOI:10.1007/s11663-016-0816-5.
23. Wang, J. Zhang, Y. Sasaki, O. Ostrovski, C. Zhang and D. Cai, *Proceedings of the 10th International Conference on Molten Slags, Fluxes and Salts*, TMS, Seattle, 2016.
24. V. Stolyarova: *Open Thermodyn. J*., 2013, vol. 7, pp. 57–70.
25. Y. Kashiwaya, C.E. Cicutti, A.W. Cramb, and K. Ishii: *ISIJ Int*., 1998, vol. 38, pp. 348–56.
26. K.C. Mills: *ISIJ Int*., 1993, vol. 33, pp. 148–55.
27. Y.Q. Sun and Z.T. Zhang: *Metall. Mater. Trans. B*, 2015, vol. 46, pp. 1549–54.
28. X.H. Huang, J.L. Liao, K. Zheng, H.H. Hu, F.M. Wang, and Z.T. Zhang: *Ironmak Steelm*., 2014, vol. 41, pp. 67–74.
29. M. Asano and Y. Yasue: *J. Nucl. Mater*., 1986, vol. 138, pp. 65–72.
30. ET Turkdogan: *Physical Chemistry of High Temperature Technology*, Academic Press, New York, 1980.
31. B. Mysen: *Eur. J. Mineral*., 2003, vol. 15, pp. 781–802.
32. J. Szekely and N.J. Themelis: *Rate Phenomena in Process Metallurgy*, 1st ed., Wiley-Interscience, New York, 1971.
33. R.B. Bird, W.E. Stewart, and E.N. Lightfoot: *Transport Phenomena*, 1st ed., Wiley, New York, 2007.
34. J.D. Mackenzie: *Trans. Faraday Soc*., 1956, vol. 52, pp. 1564–68.
35. K. Shimizu and Ph.D. Dissertation: *Carnegie Mellon University*, Pittsburgh, Pensylvania, 1998.
36. G. Kolykov, *Stroenie stekla*, *Proceedings of the Conference on Glass Structure*, pp. 234–244, 1955.